International Journal of Mass Spectrometry 473 (2022) 116792

Contents lists available at ScienceDirect

International Journal of Mass Spectrometry

journal homepage: www.elsevier.com/locate/ijms

Thermochemical and conformational studies of Ni(II) and Zn(II) ternary complexes of alternative metal binding peptides with nitrilotriacetic acid

Amber A. Flores [a], Anna V. Arredondo [a], Anna J. Corrales [a], Chloe L. Duvak [a], Charles L. Mitchell [a], Oladapo Falokun [a], Cynthia L. Aguilar [a], Aram Kim [a], Bency C. Daniel [a], H. Derya Karabulut [a], Riccardo Spezia [b], Laurence A. Angel [a, *]

[a] Department of Chemistry, Texas A&M University-Commerce, 2600 S Neal Street, Commerce, TX, 75428, USA
[b] Laboratoire de Chimie Théorique, Sorbonne Université, UMR 7616 CNRS, 4, Place Jussieu, 75005, Paris, France

ARTICLE INFO

Article history:
Received 24 September 2021
Received in revised form
14 November 2021
Accepted 29 December 2021
Available online 4 January 2022

Keywords:
Threshold collision-induced dissociation
Energy-resolved CID
Metal(II)-NTA-Peptide ternary complexes
Immobilized metal affinity chromatography
Peptide tags

ABSTRACT

Energy-resolved threshold collision-induced dissociation (TCID) of negatively-charged [amb$_5$-H+M(II)+NTA-2H]$^-$ ternary complexes were studied for how they competitively dissociated into the products [amb$_5$-3H+*M*(II)]$^-$ + NTA or [NTA-3H+*M*(II)]$^-$ + amb$_5$, where *M* = Zn or Ni and NTA is nitrilotriacetic acid. The complexes contained one of the alternative metal binding-5 (amb$_5$) heptapeptides with primary structures acetyl-Aa$_1$-Aa$_2$-Gly$_3$-Pro$_4$-Tyr$_5$-Aa$_6$-Aa$_7$, where the amino acids Aa$_{1,2,6,7}$ included the potential metal binding sites of Asp, His, and/or Cys. The study included heptahistidine which represents the His affinity tag commonly used in immobilized metal affinity chromatography (IMAC) separation of recombinant proteins. Molecular modeling using PM6 located low energy, geometry-optimized conformers of the ternary complexes and their products which had collision cross sections that agreed with those measured by ion mobility. Using the molecular parameters, including vibrational and rotational frequencies, of the reactant and products from the molecular modeling, the energy-dependent intensities of the two product channels were modeled using a competitive TCID method to determine their threshold energies which equated to the two product channels 0 K dissociation enthalpies (ΔH_0). Statistical mechanics thermal corrections provided the 298 K enthalpies (ΔH_{298}) and Gibbs free energies (ΔG_{298}) for the association reactions [amb$_5$-3H+*M*(II)]$^-$ + NTA ↔ [amb$_5$-H+*M*(II)+NTA-2H]$^-$ and [NTA-3H+*M*(II)]$^-$ + amb$_5$ ↔ [amb$_5$-H+*M*(II)+NTA-2H]$^-$. These results were compared to determine which amb$_5$ were effective as alternative tags for IMAC purification of recombinant proteins and is a routine that can be generally applied to compare the thermochemistry of metal ion ternary complexes.

1. Introduction

For the purification of recombinant proteins, the gene coding for a specific protein is spliced into a bacteria's plasmid. The bacteria then produce the intended protein from the introduced gene vector, but also continue to produce their natural proteins. This creates a mixture of proteins in which the intended recombinant protein must be separated and purified using a His-tag through the immobilized metal ion affinity chromatography (IMAC) procedure [1]. The IMAC method includes a metal stationary phase within a column derivatized with nitrilotriacetic acid (NTA), the utilized chelating agent that immobilizes the metal ions. As the protein mixture passes through the column, the intended recombinant proteins with the His-tag will bind to the metal sites and are captured within the column. Any untagged proteins will run through the column and wash out. The final collection of the retained His-tagged proteins requires the column to be washed with imidazole buffer or a pH gradient that displaces the protein from the column [2,3].

The results described here focus on seven heptapeptide sequences previously studied [4] that showed the potential as alternative metal binding-5 (amb$_5$) tags: **A**, **H**, **I**, **J**, **N**, **O** and **P** (Fig. 1), where **P** is the His-tag control to which the results of the

* Corresponding author. Department of Chemistry, Texas A&M University-Commerce, 2600 S Neal St., Commerce, TX, 75428, USA.
E-mail address: Laurence.Angel@tamuc.edu (L.A. Angel).

https://doi.org/10.1016/j.ijms.2021.116792
1387-3806/

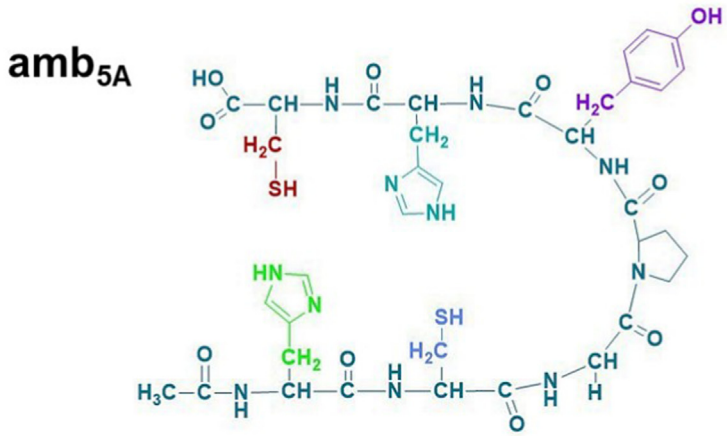

A ac-His_1-Cys_2-Gly_3-Pro_4-Tyr_5-His_6-Cys_7-OH
H ac-Asp_1-Cys_2-Gly_3-Pro_4-Tyr_5-His_6-Cys_7-OH
I ac-Asp_1-Asp_2-Gly_3-Pro_4-Tyr_5-His_6-Cys_7-OH
J ac-Asp_1-Asp_2-Gly_3-Pro_4-Tyr_5-His_6-Asp_7-OH
N ac-Asp_1-Cys_2-Gly_3-Pro_4-Phe_5-His_6-Cys_7-OH
O ac-His_1-His_2-Gly_3-Pro_4-Tyr_5-His_6-His_7-OH
P ac-His_1-His_2-His_3-His_4-His_5-His_6-His_7-OH

Fig. 1. The alternative metal binding-5 peptides **A**, **H**, **I**, **J**, **N**, **O**, and **P** showing their primary structures with colors designating the residues changed at positions 1, 2, 5, 6 and 7.

electrospray - ion mobility - mass spectrometry (ESI-IM-MS) study of the other six amb_5 tags were compared. The tested $[amb_5\text{-}H{+}M(II){+}NTA\text{-}2H]^-$ ternary complexes, where NTA = nitrilotriacetic acid and M = Zn(II) or Ni(II), represent the peptide-metal-ligand complex formed in an IMAC column. The intention of the study is to determine an amb_5 tag that exhibits similar characteristics to the commercially used His-tag but overcomes the issues of stability, aggregation and toxicity exhibited in some His-tag applications [1,5,6]. The amb_5's heterogeneous primary structures and their increased hydrophilicities over the His-tag may overcome these issues.

The pH-dependent behavior of the amb conformers can be examined by ESI-IM-MS as shown by our previous studies [4,7–14]. The amb_5 peptides have shown their Ni(II) and Zn(II) complexes form at pH $\geq$ 7, an important attribute for their potential in applications as affinity tags, because pH can be used to control their metal affinity in the IMAC column [4,10,12,14]. Their primary structure has a pair of metal binding His, Cys, and/or Asp side groups at either terminal of the peptide (Fig. 1) and three central residues that act as: (1) Gly_3, a spacer, (2) Pro_4, a hinge, and (3) Tyr_5, a source of π-metal cation and hydrogen bonding.

The results of the collision-induced dissociation (CID) of selected $[amb_5\text{-}H{+}M(II){+}NTA\text{-}2H]^-$ ternary complexes are reported here. Early CID studies of peptides included that of Gross et al. [15] who investigated the structure of the amino acid sequence of the toxin *Helminthosporium carbonum* using fast atom bombardment (FAB) to desorb the protonated cyclic peptide. The interpretation of the CID mass spectra of the protonated peptides formed by the FAB method were also discussed in a review by Papayannopoulos [16]. Early CID experiments of ternary metal-peptide complexes included the study of Pd(II)-alanine complexes with His containing peptides [17], using ESI to generate the Pd(II) ternary complex and quadrupole ion trap (QIT) mass spectrometry to observe their CID reactions. The results showed the primary binding site of the Pd(II) was the His imidazole ring and fragmentation first took place through the dissociation of the peptide bond on the C-terminal side of His. Another QIT CID study characterized the dissociation of cyclic peptides and their metal complexes [18]. Siu and coworkers [19] studied the CID products of the ternary complexes $[Cu^{II}(Ma)(Mb)]^{2\cdot+}$, where Ma and Mb were di- or tri-peptides containing Trp or Tyr. The study showed radical formation was observed for peptide complexes including only the Trp residue, because of the low ionization energy of the Trp and electron transfer (ET) to Cu(II). The fragmentation of Tyr-containing complexes were promoted by proton transfer (PT) reactions. Competition between the ET and PT reactions were further studied in the CID studies of M^{III}(salen)−peptide complexes, where M = Co, Fe, or Mn and salen = *N,N′*-ethylene-bis(salicylideneiminato), by Laskin and coworkers [20–22].

The threshold CID (TCID) method using guided ion beam tandem mass spectrometry techniques was developed by Armentrout, Ervin and Rodgers [23]. The method includes analyses of the TCID results using a threshold law integrated over the internal energy distribution of the reactant [24], convolution over translational energy distributions between the reactant and collision gas target [25], statistical RRKM correction of the kinetic shifts resulting from the limited time window for observation of the products [26], and integration over the total rotational angular momentum J levels [27,28]. The competitive TCID method allows for the simultaneous fitting of two competing product channels [29]. These methods are

incorporated into the CRUNCH program [30] and they were used here to evaluate the dissociation of the ternary [amb$_5$-H+*M*(II)+NTA-2H]$^-$ complexes into their two main product channels, which allowed for a thermochemical analyses of these reactions.

2. Experimental section

2.1. Reagents

The amb$_5$ heptapeptides **A**, **H**, **I**, **J**, **N**, **O**, and **P** were synthesized by PepmicCo (http://www.pepmic.com/). The Zn(II) nitrate hexahydrate (99%+ purity) and Ni(II) nitrate hexahydrate (99% purity) were acquired from Alfa Aesar (www.alfa.com/) and ACROS (https://www.acros.com/), respectively. Ammonium acetate (ultrapure) and ammonium hydroxide (trace metal grade) were acquired from VWR (https://us.vwr.com/) and Fisher Scientific (http://www.Fishersci.com/), respectively. All stock and working solutions were made with deionized water >17.4 MΩ cm (http://www.millipore.com).

2.2. Preparation of the ternary complexes and ESI-IM-MS analysis

Ammonium hydroxide was added to 10.0 mM ammonium acetate to produce a pH 7.7 solution. The amb$_5$+metal+NTA complexes were prepared by combining one of the metal ions with the NTA followed by the addition a selected amb$_5$ peptide and then the ammonium acetate-ammonium hydroxide solution. The samples final concentrations were 25.0 μM for both the amb$_5$ and metal ion and 50.0 μM for NTA with 8.0 mM buffer solution. The solutions were thoroughly mixed and left at room temperature for 10 min. The solutions final pH were between pH 7.0–7.4.

2.3. Collision-induced dissociation of the [amb$_5$-H+*M*(II)+NTA-2H]$^-$ complexes

The ESI-IM-MS and CID analyses were conducted using the Waters Synapt High-Definition Mass Spectrometer (G1) [31] with a schematic (Fig. S1) and operating conditions as given in the Supporting Information. The *m/z* isotope patterns of the negatively-charged [amb$_5$-H+*M*(II)+NTA-2H]$^-$ complexes were *m/z* selected by the transmission quadrupole in resolving mode, focused into the trap where they were collected before injection into the IM traveling wave and dissociation in the transfer T-wave cell, using a predetermined range of collision energies (CE) [32]. This method allows for background dissociation of the complex not occurring at the transfer T-wave to be subtracted because only the precursor complex is ion mobility separated and products formed in the transfer T-wave cell have the same drift times, where ions formed from background CID at the entrance of the IM cell are separated and exhibit different drift times. The *m/z* of the ternary complex and its dissociation product were measured by the TOF operating in V-mode and these species were identified by matching their drift times and their *m/z* isotope patterns with theoretical isotope patterns using the Driftscope 2.0 and MassLynx 4.1 software. The area under each of the species arrival time distributions (ATDs) were integrated to determine their relative proportions and their relative abundances were calculated by normalizing their ATD area to the sum of areas of all species found at each CE. Each CID experiment were replicated 3–5 times to find the means and the standard deviations.

2.4. Collision cross sections

Collision cross sections (CCS) of the [amb$_5$-H+*M*(II)+NTA-2H]$^-$ complexes were determined by a calibration procedure that gives CCS measured in He buffer gas (Ω_{He}) allowing the comparison of their Ω_{He} to the [amb$_5$-H+*M*(II)+NTA-2H]$^-$ conformations located by the molecular modeling and their Ω_{He} calculated by the Sigma program [33]. Details of the method are described in the supporting information.

2.5. Molecular modeling of amb$_5$+M(II)+NTA conformers and their products

Geometry-optimized conformers of the negatively charged amb$_5$+*M*(II)+NTA complexes and their products were located using the semi-empirical PM6 [34] method with the Gaussian09 software [35]. Starting structures where built using our knowledge of our previously located B3LYP [36] [amb$_5$-3H+*M*(II)]$^-$ conformers [12,14], using *trans* configurations for all peptide bonds, including Pro$_4$. The potential metal binding substituent groups and the carboxylate terminus were positioned close to the metal ion to compare how PM6 would optimize the position of these ligands to coordinate the singlet or triplet spin states of Zn(II) or Ni(II), respectively. The protonation state of the lowest energy form was found to be [amb$_5$-H+*M*(II)+NTA-2H]$^-$. The enthalpy changes for the dissociation reactions of [amb$_5$-H+*M*(II)+NTA-2H]$^-$ were also calculated using PM6. For each located PM6 conformer, their Ω_{He} was computed by the Lennard-Jones (L-J) ion size scaled technique [33], using ten repeated computational measurements to determine their overall mean Ω_{He} and standard deviation, which were used to compare to the ESI-IM-MS measured Ω_{He}.

2.6. CRUNCH modeling

The lab-frame collision energy (E_{lab}) applied to the transfer collision cell was converted to the center-of-mass energy (E_{cm}) scale using the average mass of the argon (m_{Ar}) collision gas and the average mass of the ternary complex ($m_{complex}$) using:

$$E_{cm} = E_{lab}\,(m_{Ar}/(m_{Ar} + m_{complex})) \quad (1)$$

where E_{cm} represents the maximum energy from the collision with the argon gas which is converted into internal energy of the ternary complex.

The E_{cm}-dependent intensities of the two product channels [amb$_5$-H+*M*(II)+NTA-2H]$^-$ ↔ [amb$_5$-3H+*M*(II)]$^-$ + NTA and [amb$_5$-H+*M*(II)+NTA-2H]$^-$ ↔ [NTA-3H+*M*(II)]$^-$ + amb$_5$, where *M* = Zn or Ni, were modeled using the PM6 vibrational and rotational frequencies for the reactant and products using the CRUNCH program. Polarizabilities and dipole moments for the neutral species were taken either from the NIST database or the PM6 calculations.

3. Results and discussion

3.1. The threshold collision-induced dissociation of the amb$_5$+M(II)+NTA ternary complexes

The preliminary ESI-IM-MS analyses of the amb$_5$+*M*(II)+NTA ternary complexes in positive and negative ion modes showed they formed 2-, 1-, and 2+ charge states, with the 1- complex [amb$_5$-H+*M*(II)+NTA-2H]$^-$ primarily dissociating to form either the [amb$_5$-3H+*M*(II)]$^-$ or [NTA-3H+*M*(II)]$^-$ complexes (Fig. 2a). The energy-resolved CID was conducted using the Synapt's transfer T-wave cell (Fig. S1) which has been shown to be more reproducible than using the trap T-wave [12,32] because prior to dissociation the ions are thermalized by the collisions with the N_2 in the ion mobility T-wave cell. The ion energy spread was determined using retarding potential analysis (RPA) by sweeping the transfer CE

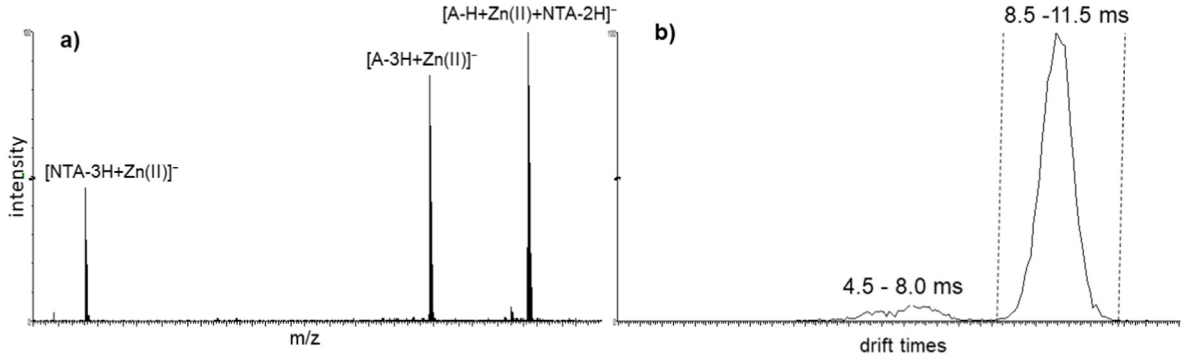

Fig. 2. The collision-induced dissociation (CID) of **a)** [amb$_{5A}$-H+Zn(II)+NTA-2H]$^-$ with 30 V transfer collision energy produced [amb$_{5A}$-3H+Ni(II)]$^-$ and [NTA-3H+Zn(II)]$^-$ with **b)** showing the resulting drift time distributions. The dashed lines show the drift time range that were used for determining the relative percent intensity of the precursor and product ions that occurred from the energy-resolved CID inside the transfer collision cell. The other labeled drift times were the products formed during the injection of the ternary complex into the entrance of the ion mobility cell.

through low voltages and monitoring the total ion current. The full width at half maximum of the derivative of the RPA curve gave a typical ion energy spread of 1.5 V lab-frame or 0.035 eV in the center-of-mass frame. The dissociation by the CE in the transfer cell can be separated from background dissociation that occurs from the initial collisions during injection of the ions into the entrance of the ion mobility cell, which is prior to ion mobility separation and complex thermalization stages. Fig. 2b shows the drift time distributions for the CID of [amb$_{5A}$-H+Zn(II)+NTA-2H]$^-$ into the [amb$_{5A}$-3H+Zn(II)]$^-$ and [NTA-3H+Zn(II)]$^-$ complexes. These drift times distributions are useful for subtracting any dissociation that occurs outside of the transfer T-wave cell because the products of the CID of [amb$_{5A}$-H+Zn(II)+NTA-2H]$^-$ inside the transfer cell will have the same drift time as their precursor ion 8.5–11.5 ms (dashed lines shown in Fig. 2b) and the formation of products before the transfer cell will have different drift time distributions (*e.g.,* 4.5–8.0 ms as shown in Fig. 2b). These were primarily due to background dissociation of the precursor at the entrance to the ion mobility cell, but the products formed here were ion mobility separated from the precursor ion as they passed down the length of the IM cell. Therefore, only the areas of the individual drift times for the precursor and product ions that were distributed between 8.5 and 11.5 ms (dashed lines) were used for the determination of the precursor and product ions percent intensity.

Tests showed that it was the trap bias setting, which controls the injection voltage of the complex ion into the ion mobility cell, which contributed to the heating and background CID of the ternary complex. The upper limit, effective temperature of the leucine enkephalin dimer, that has a similar mass to the ternary complexes studied here, was determined in the G2 Synapt instrument at the entrance of the ion mobility cell to be 449 K [37]. However, the temperature decreases as the ions pass through the IM cell resulting in Gaussian distributions in their arrival times at the TOF detector, indicating they are effectively thermalized by the low energy collisions with the N_2 gas, before their entrance into the transfer cell (Fig. S1). The trap bias setting was, therefore, set to 14 V which kept the background dissociation to a minimum but did not overly affect the overall ion count signal.

3.2. Energy-resolved collision-induced dissociation of the [amb$_5$H+M(II)+NTA-2H]$^-$ complexes

The energy-resolved CID of [amb$_5$-H+*M*(II)+NTA-2H]$^-$ complexes, where amb$_5$ = **A**, **H** or **I** and *M* = Zn or Ni (Fig. 3), show competition for forming either [amb$_5$-3H+*M*(II)]$^-$ + NTA or [NTA-3H+*M*(II)]$^-$ + amb$_5$ products, where either the amb$_5$ or NTA dissociate bound to the metal forming a negative charged species. Two main trends can be observed in Fig. 3. The first is that the [amb$_5$-3H+*M*(II)]$^-$ channel becomes more dominant over the [NTA-3H+*M*(II)]$^-$ as His$_1$ and Cys$_2$ are substituted for Asp for binding to both Ni(II) and Zn(II). The second is that the Ni(II) ternary complex of **A**, **H**, and **I** required E_{cm} = 0.31 eV–0.42 eV higher energy to reach the 50% dissociation than their Zn(II) equivalent, indicating the Ni(II) ternary complexes are more stable. The Ni(II) ternary complexes also exhibit more direct competition from both channels than the Zn(II) complexes because for Ni(II) the two channels rise from similar apparent threshold energies.

For **J** (Fig. 4 a,b) the inclusion of another Asp, *i.e.,* Asp$_7$ for Cys$_7$, results in similar behavior to **I** (Fig. 3e and f) where both ternary complexes favor the dissociation into the [amb$_5$-3H+*M*(II)]$^-$ channel over the [NTA-3H+*M*(II)]$^-$ channel. The comparison of **I** to **J** shows a small decrease in the 50% dissociation for **I** and a switching of the intensities of [NTA-3H+Ni(II)]$^-$ and the minor channel [amb$_5$-3H-H$_2$O+Ni(II)]$^-$ which is the loss of H$_2$O from the [amb$_5$-3H+Ni(II)]$^-$ main channel (Figs. 3f and 4b). The change to the 4His motif of **O** (Fig. 4c and d) results with the CID favoring the formation of [NTA-3H+Ni(II)]$^-$, with the Ni(II) ternary complex requiring E_{cm} = 0.18 eV higher collision energy to reach 50% dissociation over the Zn complex. The 7xHis-tag, **P**, shows both product channels rising from an apparent similar threshold, with the [NTA-3H+*M*]$^-$ becoming the dominant product at higher collision energies. Again, as with the other ambs, the Ni(II) ternary complex requires higher collision energy (E_{cm} = 0.19 eV) to dissociate the complex 50%. The CID of the ternary complex of **N** (Fig. S14) showed a similar result to **H** (Fig. 3c and d) for the two main product channels, explained because the only difference in their primary structures are the Phe$_5$ or Tyr$_5$, respectively. However, the CID of the Zn(II) ternary complex of **N** did not produce the minor [amb$_5$-3H-H$_2$O+Zn(II)]$^-$ channel, indicating the loss of H$_2$O from **H** was from the hydroxyl group of Tyr. Also, the CID of the Ni(II) ternary complex of **N** produced the minor [NTA-CO$_2$]$^-$ channel. The 50% dissociation energies for both Zn(II) and Ni(II) ternary complexes of **N** were E_{cm} = 0.04–0.05 eV less than for equivalent complexes for **H**.

3.3. Conformers of [amb$_5$-H+M(II)+NTA-2H]$^-$ complexes and their collision cross sections

Our previous studies [4,12,14] located geometry-optimized Zn(II) and Ni(II) complexes of the amb$_5$ peptides where the primary ligands were the substituent groups of Aa$_1$-Aa$_2$-Aa$_7$ residues with the carboxyl terminus. The conformer's L-J CCS$_{He}$ all agreed

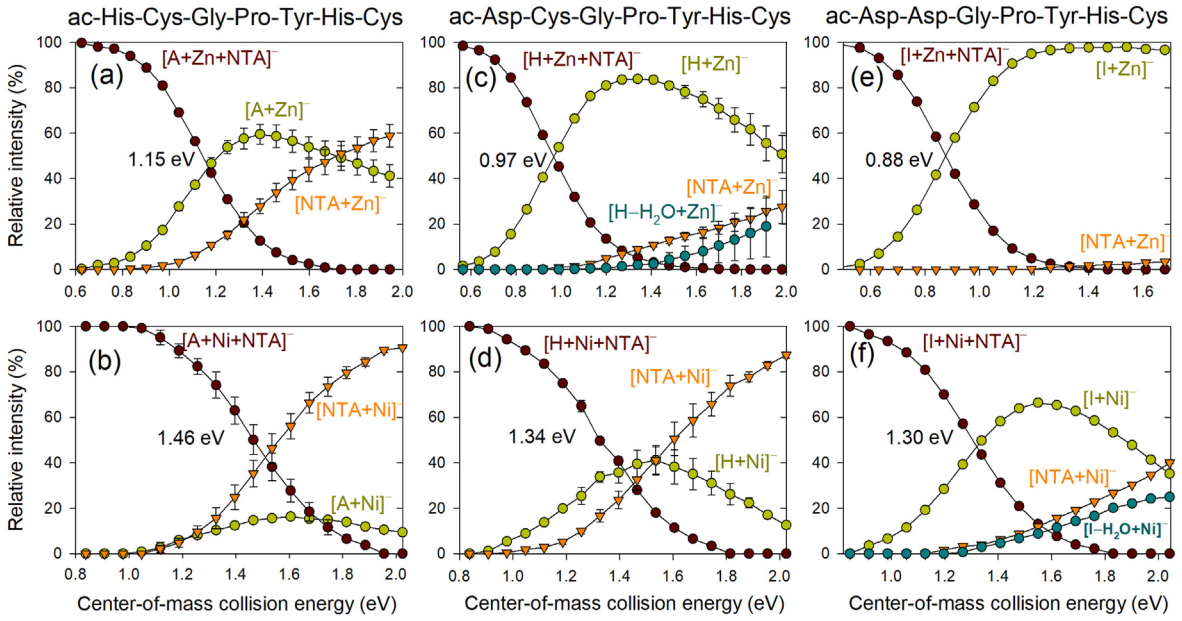

Fig. 3. The energy-resolved (c.m./eV) collision-induced dissociation of $[amb_5\text{-H}+M(II)+NTA\text{-}2H]^-$ for **A**, **H**, and **I**, where M = Zn or Ni, showing the products of $[amb_5\text{-}3H+M(II)]^-$, $[NTA\text{-}3H+M(II)]^-$ and $[amb_5\text{-}3H\text{-}H_2O+M(II)]^-$. The energy (eV) values shown on the graphs are where there is 50% dissociation of the $[amb_5\text{-H}+M(II)+NTA\text{-}2H]^-$ complex.

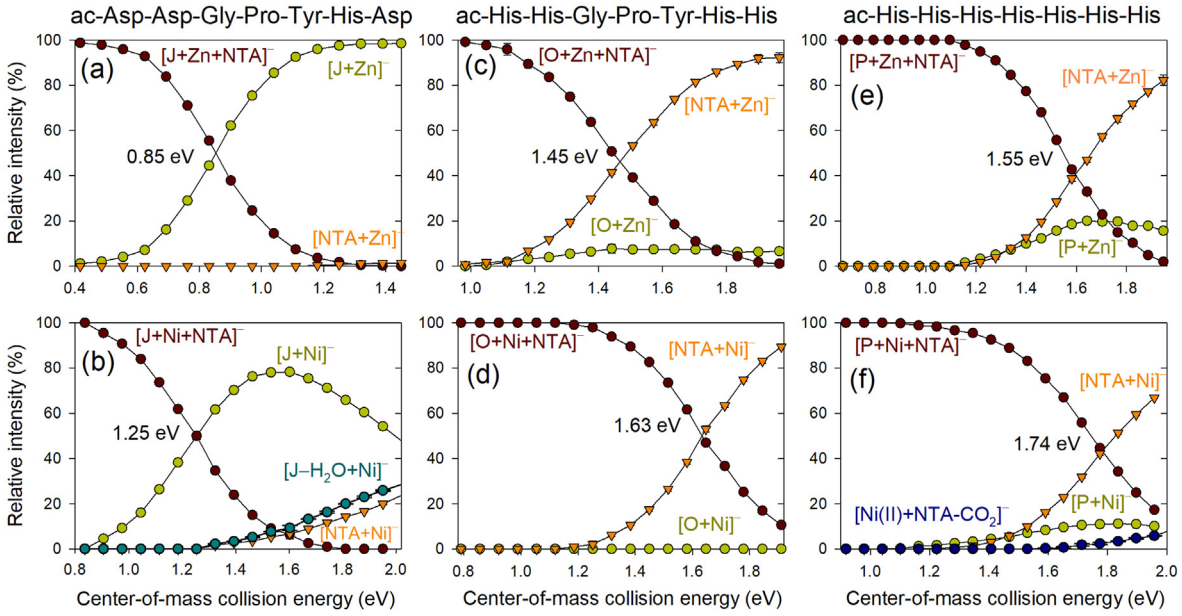

Fig. 4. The energy-resolved (c.m./eV) collision-induced dissociation of $[amb_5\text{-H}+M(II)+NTA\text{-}2H]^-$ for **J**, **O**, and **P**, where M = Zn or Ni, showing the products of $[amb_5\text{-}3H+M(II)]^-$, $[NTA\text{-}3H+M(II)]^-$ and $[amb_5\text{-}3H\text{-}H_2O+M(II)]^-$. The energy (eV) values shown on the graphs are where there is 50% dissociation of the $[amb_5\text{-H}+M(II)+NTA\text{-}2H]^-$ complex.

with the ESI-IM-MS measured CCS_{He} for that species. These structures formed the basis for the starting structures for locating the PM6 geometry-optimized ternary complexes with the NTA.

The overall charge of the amb_5 ternary complexes are principally influenced by their His, Cys, Asp and carboxyl terminus groups and the 2+ charge of the metal ion. For example, Fig. 5 shows two examples of the PM6 geometry-optimized conformations of $[amb_{5H}\text{-H}+Zn(II)+NTA\text{-}2H]^-$ with Asp_1-Cys_7 and carboxyl terminus chelation of Zn(II) and $[amb_{5J}\text{-H}+Ni(II)+NTA\text{-}2H]^-$ with Asp_1-Asp_7 and carboxyl terminus chelation of Ni(II). The conformers for the alternative protonation states $[amb_5\text{-}2H+M(II)+NTA\text{-H}]^-$ were higher in electronic and zero point energy. The lowest-energy conformers for the other amb_5 species are shown in the supporting information Figs. S2–S13. The Aa_1-Aa_7 and carboxyl terminus were the typical binding sites for the located ternary complexes for **H**, **I**, **J** and **N** and in all cases the NTA bound the metal via the amine nitrogen and two oxygens from two carboxylate groups in a total of five or six coordinate complex. The conformers were similar and the overall charge of the ternary complexes were typically determined by the deprotonation of the Aa_1-Aa_7 substituent groups and the protonation of the His_6 imidazolium ring as shown in Fig. 5. Table 1 compares the L-J CCS_{He} of the PM6 conformations with the experimentally measured CCS_{He} by ESI-IM-MS. Good agreement is exhibited by the ternary complexes of **A**, **H**, **I**, and **J**, and there is

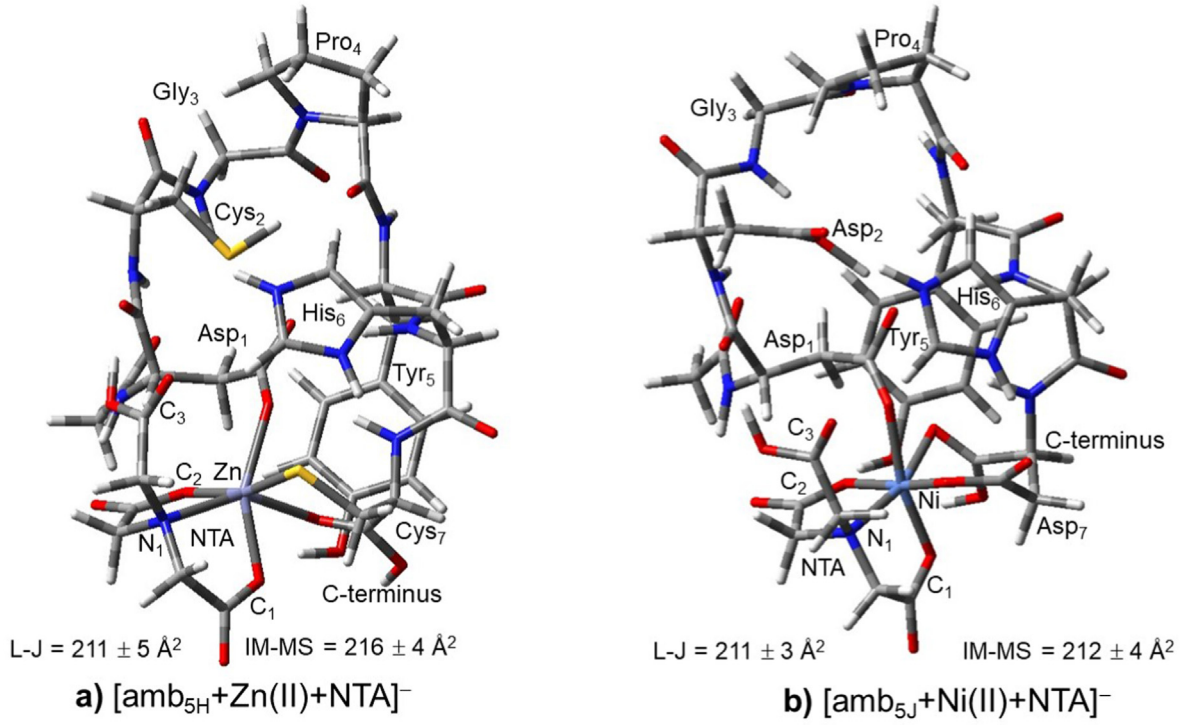

Fig. 5. The PM6 geometry-optimized ternary complexes of **a)** $[amb_{5H}\text{-}H+Zn(II)+NTA\text{-}2H]^-$ exhibiting Asp_1-Cys_7 and carboxyl terminus coordination of Zn(II) from amb_{5H} and amine (N_1) and two carboxylates (C_1 and C_2) coordination from nitrilotriacetic acid (NTA), **b)** $[amb_{5J}\text{-}H+Ni(II)+NTA\text{-}2H]^-$ exhibiting Asp_1-Asp_7 and carboxyl terminus coordination of Ni(II) from amb_{5J} and amine (N_1) and two carboxylates (C_1 and C_2) coordination from NTA. The L-J collision cross sections (CCS_{He}) for both conformers agree well to their experimentally IM-MS measured CCS_{He}.

Table 1
Collision cross sections (Å^2) from PM6 theory and ESI-IM-MS experiments.

amb_5	$[amb_5\text{-}H + Zn(II)+NTA\text{-}2H]^-$		$[amb_5\text{-}H + Ni(II)+NTA\text{-}2H]^-$	
	PM6	Exp.[a]	PM6	Exp.[a]
A	214 ± 2	214	219 ± 2	218
H	211 ± 5	216	212 ± 3	215
I	216 ± 4	217	216 ± 3	212
J	212 ± 4	217	211 ± 3	212
N	211 ± 3	222	211 ± 3	220
O	243 ± 4	230	246 ± 4	230
P	262 ± 5	240	261 ± 6	241

[a] ESI-IM-MS CCS_{He} measurements have uncertainties of ±4 Å^2.

Table 2
Metal coordination bond lengths (Å) for the PM6 conformers of the $[amb_{5H}\text{-}H+Zn(II)+NTA\text{-}2H]^-$ and $[amb_{5J}\text{-}H+Ni(II)+NTA\text{-}2H]^-$ ternary complexes.

Bonds	$[amb_{5H}\text{-}H+Zn(II)+NTA\text{-}2H]^-$	$[amb_{5J}\text{-}H+Ni(II)+NTA\text{-}2H]^-$
Asp_1–M(II)	2.192	2.100
Aa_7–M(II)	2.311	2.004
C-term–M(II)	2.288	2.021
NTA C_1–M(II)	2.101	1.976
NTA C_2–M(II)	2.047	2.000
NTA N_1–M(II)	2.256	1.958

reasonable agreement for **N**. The **O** and **P** species with 4 and 7 His residues have L-J CCS_{He} that are greater than the ESI-IM-MS measured CCS_{He}. This was related to the PM6 predicted steric hindrance of the bulky His imidazole groups, which resulted in conformers for **O** and **P** exhibiting only 1 or 2 His side groups binding to the metal ion, respectively, with some His forming hydrogen bonds but other His not contributing to intramolecular interactions, resulting in more extended conformers especially for **P**.

Fig. 5 shows the Asp_1 and Cys_7 or Asp_7 substituent groups and the carboxyl terminus coordinate the metal ion along with the NTA also deprotonated at two carboxylate groups contributing to the overall charge of -1 of the ternary complex. The measured L-J CCS_{He} for both conformers are in good agreement with their experimentally measured IM-MS CCS_{He}, as shown in Fig. 5, which give further support of the existence of these conformers. Table 2 compares the bond lengths for the coordination sites in the **H** and **J** ternary complexes. For the Ni(II) ternary complex of **J**, each bond length is shorter than the equivalent bond length for the Zn(II) complex of **H**. The predicted tighter coordination of Ni(II) coincides with the higher collision energies required for 50% dissociation of the Ni(II) complexes over the Zn(II) complexes as shown in Figs. 3 and 4.

3.4. Energy-resolved collision-induced dissociation of the $[amb_5\text{-}H+M(II)+NTA\text{-}2H]^-$ complexes

The thermochemical analysis using the threshold CID values (Tables 3 and 4) were determined by modeling the energy-dependent intensities of the two product channels using the CRUNCH program [23]. The method includes the internal energy distribution of the ternary complex [24], convolution over translational energy distributions between the ternary complex ion and the argon collision gas [25], statistical RRKM correction of the kinetic shifts due to the 50 μs time window from the collision cell to the TOF detector [26], integration over the total rotational angular momentum J levels [27,28], and the competitive shift from the two competing channels [29]. The de-convoluted CRUNCH model relates the 0 K threshold energy (Figs. 6 and 7) to the 0 K enthalpies of

Table 3
Comparison of the energy-resolved CID modeled using the CRUNCH program and the PM6 dissociation enthalpies (ΔH_0) at 0 K for the reactions $[amb_5\text{-H}+M(II)+NTA\text{-}2H]^- \leftrightarrow [amb_5\text{-}3H+M(II)]^- + NTA$ and $[amb_5\text{-H}+M(II)+NTA\text{-}2H]^- \leftrightarrow [NTA\text{-}3H+M(II)]^- + amb_5$, where M = Zn or Ni. Values are in kJ/mol.

	$[amb_5\text{-H}+Zn(II)+NTA\text{-}2H]^-$				$[amb_5\text{-H}+Ni(II)+NTA\text{-}2H]^-$			
	$[amb_5\text{-}3H+Zn(II)]^-$		$[NTA\text{-}3H+Zn(II)]^-$		$[amb_5\text{-}3H+Ni(II)]^-$		$[NTA\text{-}3H+Ni(II)]^-$	
amb_5	CID	PM6	CID	PM6	CID	PM6	CID	PM6
A	118	131	149	200	146	135	148	122
H	98.2	62.3	147	167	125	157	161	111
I	107	98.7	–	218	112	169	158	134
J	114	136	–	179	130	243	195	130
N	92.0	88.2	133	153	112	233	169	138
O	85.7	136	128	212	–	209	130	195
P	127	195	132	123	117	122	161	79.6

dissociation for the two reactions:

$$[amb_5\text{-H}+M(II)+NTA\text{-}2H]^- \leftrightarrow [amb_5\text{-}3H+M(II)]^- + NTA \quad (2)$$

$$[amb_5\text{-H}+M(II)+NTA\text{-}2H]^- \leftrightarrow [NTA\text{-}3H+M(II)]^- + amb_5 \quad (3)$$

where M = Zn or Ni (Table 3). For example, the dissociation of the Zn(II) ternary complex of **A** (Fig. 6a), the formation of the $[amb_{5A}\text{-}3H + Zn(II)]^-$ product exhibited a 0 K threshold energy of 1.32 eV which equated to the dissociation enthalpy for reaction 2. The relative intensities of this channel rose to about 58% intensity before the $[NTA\text{-}3H+Zn(II)]^-$ channel became apparent, exhibiting a 0 K threshold energy of 1.54 eV for reaction 3. The dissociation of the analogous Ni(II) ternary complexes of **A** (Fig. 6b), showed reactions 2 and 3 exhibited threshold energies of 1.52 eV and 1.54 eV, respectively, with the $[NTA\text{-}3H+Ni(II)]^-$ intensities rising to 90% by 2.0 eV. The ΔH_0 for reaction 2, therefore, was 0.20 eV higher for the Ni(II) complex over the Zn(II) complex explaining the higher 50% breakdown energy of the Ni(II) ternary complex shown in Fig. 3a and b.

For the two ternary complexes of **H** (Fig. 6c and d) the dissociation of the Zn(II) ternary complex exhibited 0 K threshold energies of 0.997 eV and 1.52 eV for reactions 2 and 3, respectively, both lower than the 1.30 eV and 1.67 eV for the analogous reactions from the Ni(II) ternary complex. For **I**, the dissociation of the Zn(II) ternary complex primarily produced the 0 K threshold energy of 1.11 eV for reaction 2 and at higher energies a weak signal for reaction 3 that could not be fitted satisfactorily. The analogous Ni(II) ternary complex of **I** exhibited a greater competition between the two channels; 1.16 eV and 1.64 eV for reactions 2 and 3, respectively.

The CRUNCH fitting of **J**, **O**, and **P** (Fig. 7) shows for **J** (Fig. 7a and b) the Zn(II) ternary complex exhibited 0 K threshold energy of 1.18 eV for reaction 2, while for the analogous Ni(II) ternary complex exhibited 1.34 eV and 2.02 eV for reactions 2 and 3, respectively. For **O** where the potential binding sites were 4His, reaction 3 became the principal product channel, with the Zn(II) complex exhibiting 0.888 eV and 1.33 eV for reactions 2 and 3 respectively, while the Ni(II) ternary complex exhibited 1.34 eV for only reaction 3. For **P**, the 7xHis-tag, the product channels were in competition; with the Zn(II) ternary complex exhibiting 1.32 eV for reaction 2 and 1.37 eV for reaction 3, while the Ni(II) complex exhibited 1.21 eV and 1.67 eV for reactions 2 and 3, respectively. The threshold fits of the Zn(II) ternary complex of **N** (Fig. S15), gave 0.953 eV for reaction 2 and 1.38 eV for reaction 3, while the Ni(II) complex gave 1.16 eV and 1.76 eV for reactions 2 and 3, respectively.

3.5. Enthalpies (ΔH_0) of dissociation from the CID threshold measurements and PM6 molecular modeling

Table 3 compares the ΔH_0 for reactions 2 and 3 (converted to kJ/mol) from the threshold CRUNCH fitting and the electronic and zero point energies of the reactants and products located by the geometry-optimizations by PM6. For the dissociation of the Zn(II) ternary complex, PM6 agrees with the CID threshold measurements that reaction 2 has a lower ΔH_0 than reaction 3 for all the amb_5 species apart from **P**. The Zn(II) complexes of **A**, **H**, **I**, **J**, and **N** also exhibit the similar trends in ΔH_0 between CID and PM6 for reaction 2. However, for the Ni(II) complexes PM6 predicts reaction 2 has the higher ΔH_0, whereas, the CID thresholds predict the higher ΔH_0 are for reaction 3. There are also no obvious similarities in the trends of ΔH_0 between CID and PM6. For the threshold CID, the individual ΔH_0 values may have relative uncertainties of between 10 and 50% [38], however, the uncertainties in the difference in ΔH_0 between the two reactions 2 and 3 will not significantly change their order, indicating the PM6 results are in reasonable agreement with the CID for the Zn(II) complexes but systematically over estimates ΔH_0 for reaction 2 or under estimates reaction 3 for the Ni(II) complexes.

Table 4
Thermochemical analysis of the energy-resolved CID used to calculate enthalpies (ΔH_{298}) of association and Gibbs free energies (ΔG_{298}) of association at 298 K for the reactions $[amb_5\text{-}3H+M(II)]^- + NTA \leftrightarrow [amb_5\text{-H}+M(II)+NTA\text{-}2H]^-$ and $[NTA\text{-}3H+M(II)]^- + amb_5 \leftrightarrow [amb_5\text{-H}+M(II)+NTA\text{-}2H]^-$, where M = Zn or Ni. Values are in kJ/mol. The loss of three protons (-3H) in the table are not shown.

	$[amb_5+Zn(II)]^- + NTA$		$[NTA+Zn(II)]^- + amb_5$		$[amb_5+Ni(II)]^- + NTA$		$[NTA+Ni(II)]^- + amb_5$	
amb_5	ΔH_{298}	ΔG_{298}	ΔH_{298}	ΔG_{298}	ΔH_{298}	ΔG_{298}	ΔH_{298}	ΔG_{298}
A	−127	−34.0	−182	−21.8	−171	−45.7	−154	−53.1
H	−99.5	−28.3	−170	−44.7	−140	−47.0	−216	−31.1
I	−128	−12.0	–	–	−114	−42.9	−206	−31.9
J	−138	−10.6	–	–	−134	−49.2	−251	−37.1
N	−93.1	−22.5	−136	−51.1	−113	−43.9	−221	−13.1
O	−86.8	−20.8	−138	−47.6	–	–	−133	−55.5
P	−131	−40.7	−133	−46.9	−120	−35.5	−163	−79.1

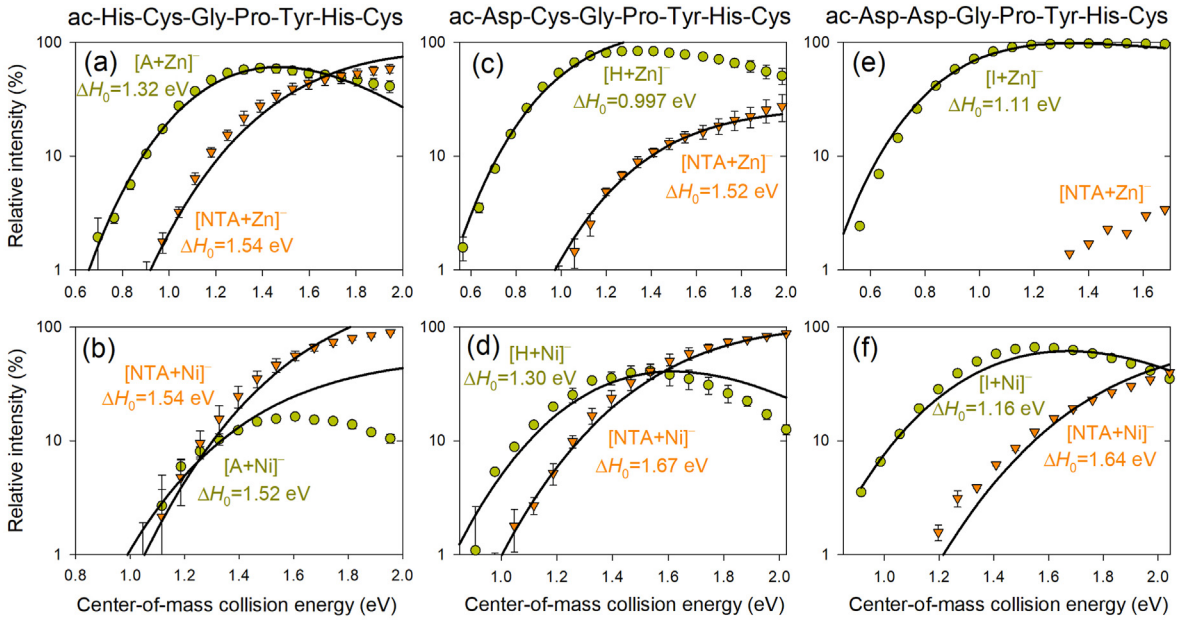

Fig. 6. The energy-resolved collision-induced dissociation of [amb$_5$-H+*M*(II)+NTA-2H]$^-$ for **A**, **H**, and **I**, where *M* = Zn or Ni, showing the products of [amb$_5$-3H+*M*(II)]$^-$ and [NTA-3H+*M*(II)]$^-$ with the CRUNCH threshold fits. The energy (eV) values shown are the dissociation enthalpies (ΔH_0) at 0 K for the reactions [amb$_5$-H+*M*(II)+NTA-2H]$^-$ ↔ [amb$_5$-3H+*M*(II)]$^-$ + NTA and [amb$_5$-H+*M*(II)+NTA-2H]$^-$ ↔ [NTA-3H+*M*(II)]$^-$ + amb$_5$.

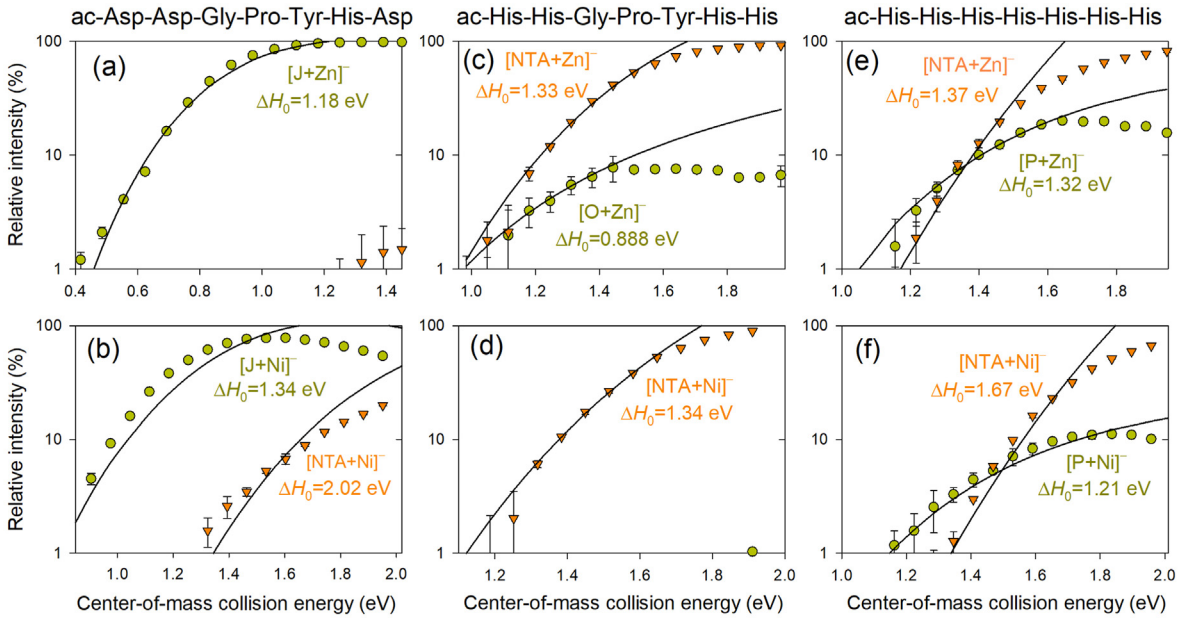

Fig. 7. The energy-resolved collision-induced dissociation of [amb$_5$-H+*M*(II)+NTA-2H]$^-$ for **J**, **O**, and **P**, where *M* = Zn or Ni, showing the products of [amb$_5$-3H+*M*(II)]$^-$ and [NTA-3H+*M*(II)]$^-$ with the CRUNCH threshold fits. The energy (eV) values shown are the dissociation enthalpies (ΔH_0) at 0 K for the reactions [amb$_5$-H+*M*(II)+NTA-2H]$^-$ ↔ [amb$_5$-3H+*M*(II)]$^-$ + NTA and [amb$_5$-H+*M*(II)+NTA-2H]$^-$ ↔ [NTA-3H+*M*(II)]$^-$ + amb$_5$.

3.6. Thermochemical analysis of enthalpies (ΔH_{298}) and Gibbs free energies (ΔG_{298}) of association

Considering the reverse directions of reactions 2 and 3 allows the enthalpies (ΔH_{298}) and Gibbs free energies (ΔG_{298}) of association to be determined (Table 4). These values are derived from the CID ΔH_0 measurements from Table 3 with statistical mechanics thermal corrections using the PM6 rotational and vibrational frequencies for the reactants and products. The reverse of reaction 3 is of particular interest as it is the association of the amb tag with the NTA metal ion complex, a reaction that represents the tagged recombinant protein binding to the NTA immobilized metal ion inside the IMAC column. Table 4 shows the ΔH_{298} for these reverse reactions are generally more exothermic for reaction 3 than reaction 2, apart for **A** whose ΔH_{298} was greater for reaction 2 for the formation of the Ni(II) ternary complex. The amb$_5$ **H**, **I**, **J**, and **N** exhibited the greatest exothermicities for the reverse of reaction 3 with Ni(II), but were disfavored more entropically than **A**, **O**, and **P** which exhibited the most spontaneous ΔG_{298}. These previous two groups are distinguished by having either one of more Asp in their

primary structure, including Asp_1, or multiple His, including His_1. The ΔG_{298} for the reverse reactions 2 and 3 are also greater in their magnitudes of spontaneity for the Ni(II) complexes over the equivalent Zn(II) complexes, apart from **P** for reaction 2 and **H** and **N** for reaction 3, indicating the amb_5 peptides generally form the Ni(II) ternary complexes more spontaneously.

4. Conclusions

The energy-resolved CID of the ternary complexes $[amb_5\text{-}H+M(II)+NTA\text{-}2H]^-$, where amb_5 was one of the heptapeptides **A**, **H**, **I**, **J**, **N**, **O**, or **P**, produced the dissociation reactions $[amb_5\text{-}H+M(II)+NTA\text{-}2H]^- \leftrightarrow [amb_5\text{-}3H+M(II)]^- + NTA$ and $[amb_5\text{-}H+M(II)+NTA\text{-}2H]^- \leftrightarrow [NTA\text{-}3H+M(II)]^- + amb_5$. The reactions exhibited competition between either the NTA or amb_5 remaining complexed to the Zn(II) or Ni(II). Molecular modeling with geometry-optimizations of the reactants and products of these two reactions allowed for the thermochemical analysis of the reactions using explicit consideration of the energetics of the reactants, activated complexes, and products using the CRUNCH reaction dynamics program [23]. The results showed that the Ni(II) ternary complexes generally exhibited higher dissociation threshold energies than their Zn(II) counterparts and the thermochemistry of the reverse reactions gave spontaneous ΔG_{298} for the formation of the $[amb_5\text{-}H+Ni(II)+NTA\text{-}2H]^-$ ternary complexes, especially those for **A**, **O**, and **P**, where **P** is the commonly used 7xHis-tag. The results indicate the amb_5 peptides have potential as recombinant protein fusion tags for the Ni(II) IMAC method. The molecular modeling showed the amb_5 peptides **H**, **I**, **J**, and **N** principally coordinated the Zn(II) or Ni(II) via their Aa_1, Aa_7 and carboxyl terminus sites, whereas the NTA bound to the metal ion via oxygens from two carboxylate groups and the nitrogen from the amine group in a total of a 6 coordinate conformation of the ternary complex. All the amb_5 species that contained Asp also exhibited spontaneous ΔG_{298} for the formation of Zn(II) and Ni(II) ternary complexes. However, the greater spontaneity for the formation of the $[amb_5\text{-}H+Ni(II)+NTA\text{-}2H]^-$ complex from $[NTA\text{-}3H+Ni(II)]^- + amb_5$ by **A** and **O** suggests that binding via the Aa_7 sites of Cys_7 or His_7 with the carboxyl terminus was entropically more favorable. The molecular modeling indicated that the Cys or Asp substituent sites could coordinate the metal ion most effectively with little steric hindrance, commonly forming 6 coordinate ternary complexes, whereas, the species **O** and **P** with multiple imidazoles of His were sterically hindered, resulting in 5 coordinate complexes which may have dynamical implications for the formation of their ternary complexes.

Author statement

All data in this article is available by contacting the corresponding author.

Declaration of competing interest

The authors declare that they have no known competing financial interests or personal relationships that could have appeared to influence the work reported in this paper.

Acknowledgements

This material is based upon work supported by the National Science Foundation under 1764436, NSF REU program (CHE-1659852), NSF instrument support (MRI-0821247), Welch Foundation (T-0014), and computing resources from the Department of Energy (TX-W-20090427-0004-50) and L3 Communications. We thank Kent M. Ervin (University of Nevada - Reno) and Peter B. Armentrout (University of Utah) for sharing the CRUNCH program and advice on fitting from PBA. We also thank Michael T. Bowers (University of California - Santa Barbara) for sharing the Sigma program.

Appendix A. Supplementary data

Supplementary data to this article can be found online at https://doi.org/10.1016/j.ijms.2021.116792.

References

[1] C. Amarasinghe, J.-P. Jin, Protein Pept. Lett. 22 (2015) 885–892.
[2] J.A. Bornhorst, J. Falke, J. Methods Enzymol. 326 (2000) 245–254.
[3] A. Spriestersbach, J. Kubicek, F. Schaefer, H. Block, B. Maertens, Methods Enzymol. 559 (2015) 1–15.
[4] A.A. Flores, O.S. Falokun, A.B. Ilesanmi, A.V. Arredondo, L. Truong, N. Fuentes, R. Spezia, L.A. Angel, Int. J. Mass Spectrom. 463 (2021), 116554.
[5] W.T. Booth, C.R. Schlachter, S. Pote, N. Ussin, N.J. Mank, V. Klapper, L.R. Offermann, C. Tang, B.K. Hurlburt, M. Chruszcz, ACS Omega 3 (2018) 760–768.
[6] F. Khan, P.M. Legler, R.M. Mease, E.H. Duncan, E.S. Bergmann-Leitner, E. Angov, Biotechnol. J. 7 (2012) 133–147.
[7] R. Sesham, D. Choi, A. Balaji, S. Cheruku, C. Ravichetti, A.A. Alshahrani, M. Nasani, L.A. Angel, Eur. J. Mass Spectrom. 19 (2013) 463–473.
[8] D. Choi, A.A. Alshahrani, Y. Vytla, M. Deeconda, V.J. Serna, R.F. Saenz, L.A. Angel, J. Mass Spectrom. 50 (2015) 316–325.
[9] Y. Vytla, L.A. Angel, Anal. Chem. 88 (2016) 10925–10932.
[10] S.M. Wagoner, M. Deeconda, K.L. Cumpian, R. Ortiz, S. Chinthala, L.A. Angel, J. Mass Spectrom. 51 (2016) 1120–1129.
[11] E.N. Yousef, R. Sesham, J.W. McCabe, R. Vangala, L.A. Angel, JoVE (2019), e60102.
[12] Y.-F. Lin, E.N. Yousef, E. Torres, L. Truong, J.M. Zahnow, C.B. Donald, Y. Qin, L.A. Angel, J. Am. Soc. Mass Spectrom. 30 (2019) 2068–2081.
[13] A.B. Ilesanmi, T.C. Moore, L.A. Angel, Int. J. Mass Spectrom. 455 (2020), 116369.
[14] E.N. Yousef, L.A. Angel, J. Mass Spectrom. 55 (2020), e4489.
[15] M.L. Gross, D. McCrery, F. Crow, K.B. Tomer, M.R. Pope, L.M. Ciuffetti, H.W. Knoche, J.M. Daly, L.D. Dunkle, Tetrahedron Lett. 23 (1982) 5381–5384.
[16] I.A. Papayannopoulos, Mass Spectrom. Rev. 14 (1995) 49–73.
[17] V. Anbalagan, M.J. Van Stipdonk, J. Mass Spectrom. 38 (2003) 982–989.
[18] S.M. Williams, J.S. Brodbelt, J. Am. Soc. Mass Spectrom. 15 (2004) 1039–1054.
[19] Y. Ke, H.E. Aribi, C.-K. Siu, K.W.M. Siu, A.C. Hopkinson, Rapid Commun. Mass Spectrom. 24 (2010) 3485–3492.
[20] I.K. Chu, J. Laskin, Eur. J. Mass Spectrom. 17 (2011).
[21] J. Laskin, Z. Yang, C.M.D. Ng, I.K. Chu, J. Am. Soc. Mass Spectrom. 21 (2010) 511–521.
[22] J. Laskin, Z. Yang, I.K. Chu, J. Am. Chem. Soc. 130 (2008) 3218–3230.
[23] P.B. Armentrout, K.M. Ervin, M.T. Rodgers, J. Phys. Chem. 112 (2008) 10071–10085.
[24] N.F. Dalleska, K. Honma, L.S. Sunderlin, P.B. Armentrout, J. Am. Chem. Soc. 116 (1994) 3519–3528.
[25] K.M. Ervin, P.B. Armentrout, J. Chem. Phys. 83 (1985) 166–189.
[26] M.T. Rodgers, K.M. Ervin, P.B. Armentrout, J. Chem. Phys. 106 (1997) 4499–4508.
[27] V.F. DeTuri, K.M. Ervin, J. Phys. Chem. 103 (1999) 6911–6920.
[28] C. Iceman, P.B. Armentrout, Int. J. Mass Spectrom. 222 (2003) 329–349.
[29] M.T. Rodgers, P.B. Armentrout, J. Chem. Phys. 109 (1998) 1787–1800.
[30] P.B. Armentrout, K.M. Ervin, CRUNCH, Fortran Program, Version 5.2002, 2016.
[31] S.D. Pringle, K. Giles, J.L. Wildgoose, J.P. Williams, S.E. Slade, K. Thalassinos, R.H. Bateman, M.T. Bowers, J.H. Scrivens, Int. J. Mass Spectrom. 261 (2007) 1–12.
[32] U.K.B. Raja, S. Injeti, T. Culver, J.W. McCabe, L.A. Angel, Eur. J. Mass Spectrom. 21 (2015) 759–774.
[33] T. Wyttenbach, G. von Helden, J.J. Batka Jr., D. Carlat, M.T. Bowers, J. Am. Soc. Mass Spectrom. 8 (1997) 275–282.
[34] J.J.P. Stewart, J. Mol. Model. 13 (2007) 1173–1213.
[35] M.J. Frisch, G.W. Trucks, H.B. Schlegel, G.E. Scuseria, M.A. Robb, J.R. Cheeseman, G. Scalmani, V. Barone, B. Mennucci, G.A. Petersson, H. Nakatsuji, M. Caricato, X. Li, H.P. Hratchian, A.F. Izmaylov, J. Bloino, G. Zheng, J.L. Sonnenberg, M. Hada, M. Ehara, K. Toyota, R. Fukuda, J. Hasegawa, M. Ishida, T. Nakajima, Y. Honda, O. Kitao, H. Nakai, T. Vreven,

J. Montgomery, A. J, J.E. Peralta, F. Ogliaro, M. Bearpark, J.J. Heyd, E. Brothers, K.N. Kudin, V.N. Staroverov, R. Kobayashi, J. Normand, K. Raghavachari, A. Rendell, J.C. Burant, S.S. Iyengar, J. Tomasi, M. Cossi, N. Rega, J.M. Millam, M. Klene, J.E. Knox, J.B. Cross, V. Bakken, C. Adamo, J. Jaramillo, R. Gomperts, R.E. Stratmann, O. Yazyev, A.J. Austin, R. Cammi, C. Pomelli, J.W. Ochterski, R.L. Martin, K. Morokuma, V.G. Zakrzewski, G.A. Voth, P. Salvador, J.J. Dannenberg, S. Dapprich, A.D. Daniels, Ö. Farkas, J.B. Foresman, J.V. Ortiz, J. Cioslowski, D.J. Fox, Gaussian: Wallingford CT (2012).

[36] A.D. Becke, J. Chem. Phys. 98 (1993) 5648–5652.

[37] S.I. Merenbloom, T.G. Flick, E.R. Williams, J. Am. Soc. Mass Spectrom. 23 (2012) 553–562.

[38] L.A. Angel, K.M. Ervin, J. Phys. Chem. 110 (2006) 10392–10403.